LAWRENCE
LIVERMORE
NATIONAL
LABORATORY

UCRL-TR-233403

Electronic and Sturctural Transitions in Dense Liquid Sodium

J. Y. Raty, E. R. Schwegler, S. A. Bonev

August 7, 2007

This work was performed under the auspices of the U.S. Department of Energy by University of California, Lawrence Livermore National Laboratory under Contract W-7405-Eng-48.

Electronic and structural transitions in dense liquid sodium

Jean-Yves Raty[1], Eric Schwegler[2] & Stanimir A. Bonev[3]

[1] *FNRS-University of Liège, Sart-Tilman 4000, Belgium*

[2] *Lawrence Livermore National Laboratory, Livermore, CA 94550, USA*

[3] *Department of Physics, Dalhousie University, Halifax, NS B3H 3J5, Canada*

At ambient conditions, the light alkali metals are free-electron like crystals with a highly symmetric structure. However, they were shown recently to exhibit unexpected complexity under pressure [1-6]. It was predicted from theory [1,2] and later confirmed by experiment[3-5] that Li and Na undergo a sequence of symmetry breaking transitions driven by a Peierls mechanism. Most recently, measurements of the Na melting curve[6] revealed an unprecedented and still unexplained drop in the melting temperature from 1000 K at 30 GPa to room temperature at 120 GPa. Here we report results from *ab initio* calculations that explain the unusual melting behaviour in dense Na. We show that molten Na undergoes a series of pressure-induced structural and electronic transitions analogous to that observed in solid Na, but commencing at much lower pressure in the presence of disorder. With increasing pressure, liquid Na initially evolves by assuming a more compact local structure. However, a transition to a lower coordinated liquid takes place at a pressure around 65 GPa, accompanied by a threefold drop in electrical conductivity. A pseudogap opening at the Fermi level, an effect previously not observed in a liquid metal, drives this transition. Remarkably, the lower coordinated liquid emerges at rather elevated temperatures and above the stability

region of a closed packed free electron-like metal. We predict that similar exotic behaviour is possible in other materials as well.

The negative melting slope of Na is in a pressure range where the stable solid structures of are known to be body-centred cubic (bcc) and, above 65 GPa the more compact face centred cubic (fcc). At around 103 GPa, solid Na undergoes a Peierls distortion towards a cubic structure with a 16-atom cell (cI16 space group) [4-6] and the melting curve is reported[6] to recover a positive slope. The anomalous melting behaviour of Na suggests dramatic changes in the properties of the liquid that are of a different nature from what has been previously observed in other alkali metals. Indeed, the melting anomaly in Na is *orders of magnitude* (one in temperature and two in pressure) larger than in caesium [7,8]. A negative melting slope in caesium is caused by charge transfer, from *s* to more localized *d* states, which commences at slightly lower pressure in the liquid than in the solid [9]. Because of a lack of *d* states in the valence shell, a similar mechanism is not possible in Na. Furthermore, an analogy with the melting curve of hydrogen [10], which has also been predicted to have a negative slope above a closed packed solid, is inappropriate as well because the unusual melting behaviour of hydrogen is explained by enhanced intermolecular charge transfer in the liquid phase.

In order to investigate the structural and electronic changes in compressed Na that are responsible for the shape of its melting curve, we carry out a series of first principles molecular dynamic (FPMD) simulations between 5 and 120 GPa and up to 1500 K. First, we compute the melting curve over this pressure range. Our melting calculations are carried out in the *NVT* ensemble, where the solid phases are gradually heated until melting occurs. Although more accurate methods for melting computations exist, e.g. two-phase simulations [10,11] or free energy matching [12], the heat-until-it-melts approach employed here can be sufficient if there are no large overheating effects. This is indeed the case for Na, where the bonding properties do not change significantly upon melting

and the local order in the liquid and solid phases, as shown below, is similar. Thus, melting temperatures are computed by progressively heating the three solid structures known to be stable at room temperature up to 130 GPa, namely bcc, fcc, and cI16 [13]. The simulations are carried out with supercell sizes of 128, 108 and 128 atoms, respectively, which are sufficiently large for reproducing the Na equation of state at room temperature [4].

The melting curve obtained in this manner is shown in Fig. 1 and compared with existing experimental measurements. The computed melting temperatures (T_m) are slightly lower than the experimental data in [6] and slightly above the data in [14]. The overall agreement is remarkably good and the shape of the theoretical melting curve, in particular, closely mimics the experimental data. The agreement of the computed structure factor, $S(q)$, with measurements is also excellent. It should be noted that from our simulations we could also estimate the finite-temperature phase boundaries between bcc, fcc and cI16 (grey areas in Fig. 1). Simulations of either phase outside the indicated stability regions lead to amorphous deformations of the structures within a few picoseconds.

The first notable feature of the melting curve is the appearance of a maximum between 20 and 40 GPa and a negative slope at pressures thereafter. This turnover is above the stability region of the solid bcc phase, which according to the Clausius-Clapeyron equation indicates that structural changes in the liquid are taking place that make it denser than the bcc solid. The possibility for this occurring is not entirely surprising. In bcc each atom has eight nearest neighbours (n.n.), while in the higher-pressure fcc crystal there are 12 n.n. It is generally assumed, but rarely shown quantitatively, that molten metals exhibit similar local orders as their crystalline phases [15]. Furthermore, because finite temperature fluctuations enable structural changes in liquids to take place gradually, they may commence at lower pressures than their

analogous solid-solid transitions. This then opens up the possibility for a melting curve maximum if the sequence of solid phase transitions with increasing pressure is from less to more compact structures.

We therefore focus on identifying changes in the local order of the liquid structure along the melting curve that bear similarities with the bcc-to-fcc transition. However, to compare such a compact yet disordered local order to an ideal crystalline structure is not straightforward. In particular, we find that order parameters based on the characteristics of the first coordination shell (CS), such as pair correlation functions, angular bond distributions, Steinhard's angular cluster parameters[16], and individual neighbour distance distributions, are nearly invariant up to approximately 60GPa, as also found in another recent study [17].

Instead, we focus our examination on the second CS. Distance distribution analysis (Fig. 2A) shows that, starting at 30 GPa, the interatomic distances in the second shell decrease more rapidly with pressure compared to the first shell. In order to interpret these changes as a progressive transition from bcc to fcc-like local order, it is helpful to compare them with the interatomic distributions of finite-temperature bcc and fcc solids. Such a comparison has to be made at the same density and we have therefore employed a simplified model for finite temperature solids (Fig. 2C). The result of this comparison is that, with increasing temperature, the first CS's of bcc and fcc become almost identical. However, the 2nd CS of the heated fcc is contracted compared to the 2nd CS of the heated bcc, in exactly the same way as it is observed in the liquid between 0 and 60GPa. This model, together with the analysis of the FPMD simulations demonstrates that: (i) there are changes in the liquid structure, noticeable in the second CS, that correlate well with the shape of the melting curve; and (ii) these changes are characteristic of a transition from bcc to fcc local order at finite temperature.

The structural changes in the liquid to an fcc-like local order however cannot be used to explain the anomalous melting above 60 GPa where the solid itself assumes the close-packed fcc structure. Indeed, we observe significant structural changes above 65 GPa. These are already evident from the shapes of *g(r)* (see also Supplemental Material) and become quite clear from the neighbour distance distributions. The data in Fig. 2A, in particular, demonstrates that the first CS splits and the coordination, determined by counting the neighbour peak positions up to the first *g*(*r*) minimum, lowers from about 13 at 60 GPa down to approximately 8 at 105 GPa. The new coordination in the liquid indicates that its local order bears similarities to a distorted bcc-like structure. One such crystalline structure is cI16, which is the stable solid phase found at *much higher pressure* [4-6], namely, above 103 GPa (for a detailed description of cI16, see Hanfland *et al.* [3]). In the solid, the Peierls mechanism that stabilizes cI16 corresponds to a symmetry breaking of bcc and the appearance of a pseudogap at the Fermi level, thus lowering the electronic energy.

To confirm the parallel between molten Na and the cI16 crystal, we have computed the *S(q)* of the liquid at several pressures above the melting curve and compared it with that of the finite-temperature bcc, fcc and cI16 solids (Fig. 3A). The changes in the liquid *S(q)*, as pressure is increased, match extremely well the variations observed over the three solid phases. Just as in the cI16 crystal, the liquid structure factor above 65 GPa develops a well-pronounced shoulder next to the principle maximum and there is a phase change in the large-*q* oscillations. The parallel between liquid and solid phases is further supported by evidence in our calculations of electronic structure modifications in the liquid that drive the structural changes under pressure

(Fig. 3B). We find that the electronic density of states (DOS) of liquid and solid Na are rather similar at lower pressure (< 40 GPa) and do not deviate noticeably from the ideal bcc crystal. However, above 65 GPa, a pseudogap opens at the Fermi level in the liquid DOS that is not present in the underlying fcc solid, but is similar to the pseudogap in the high pressure cI16 crystal. As a result, the valence states in liquid Na are pushed towards lower energies; at 91 GPa, for instance, we measure a gain in band energy of 40 meV/atom in the liquid as compared to the fcc solid (see inset in Fig. 3B). This large gain in band energy is sufficient to overcome the cost in increased repulsion associated with local distortions, and the loss in entropy as compared to the non-distorted liquid. The melting temperature continues to decrease with pressure, as the modifications in the liquid progress, until the fcc to cI16 solid phase transition takes place around 100 GPa. At this point a pseudogap opens in the solid as well and the system recovers a positive slope in the melting curve.

The symmetry breaking in molten sodium is totally counterintuitive for a high-pressure and high-temperature liquid. It is clearly related to a Peierls-like mechanism, as evident by the appearance of a pseudogap together with the split of the first CS [18]. A pseudogap opening via a Peierls-like distortion has indeed been observed in simulations of semiconductor liquids, e.g. As[19], GeTe and GeSe [20], but *only at ambient pressure*, and in these cases it coincides with Peierls distortions in the underlying solids. Furthermore, the Peierls distortion observed in the stable crystalline phases of As and Sb is known to be destroyed under pressure [21], and that in GeTe and GeSe under heating [22]. Any evidence for a Peierls distortion in Sb disappears upon melting [19].

To understand why this phenomenon occurs in Na, we examine the effects of pressure and temperature on the angular momentum projections of the electronic DOS. The distortion from bcc to cI16 at 0K brings additional *p* states below the Fermi level (Fig. 4A, bottom). At low pressure, the very small lowering of the band structure

energy is not sufficient to overcome the ionic core repulsion associated with the distortion. The effect is much more pronounced at higher pressure where the interatomic distances are shorter and the formation of "bonding" *p* states is more favourable. Temperature, on the other hand, introduces disorder that results in further broadening of the *p* band and additional *p* states below the Fermi level (Fig. 4A upper lines). This is seen at finite temperature for both the solid and liquid phases. However, the inherent disorder in the liquid enables the sampling of configurations with local order similar to cI16.

These are rather general observations, which imply that similar symmetry breaking via an *s*-to-*p* transfer mechanism could be expected in other liquids. It should be borne in mind, however, that the symmetry breaking and corresponding volume decrease come at the expense of increased short-range ionic repulsion. Therefore, they are only feasible as long as these repulsions are "soft" enough so that they can be compensated by the lowering of the electronic band structure energy [18]. This is precisely the reason why similar effects in semiconductors are only observed in the low-pressure liquids of the lighter group V elements, e.g. in P and As, but not in Sb or Bi [19,23]. However, we predict that exotic liquid phases and melting behaviour is likely to be observed in other alkali and alkali-earth metals at high pressure; systems where pressure-induced electronic instabilities produce lower-symmetry crystalline phases. There is already strong evidence that similar effects exist in lithium [24].

According to these observations, the physical properties of liquid Na are expected to change in the pressure range above 60 GPa. Indeed, the electrical conductivity computed via the Kubo-Greenwood formula (Fig. 4B) shows a very strong decrease, by a factor of ~3 between 40 and 80 GPa. The conductivity curve actually deviates from the Drude shape towards a semiconductor-like shape. Though the extrapolation to zero frequency is difficult, we estimate the DC conductivity to decrease from about 32000 Ω^{-}

^{1} cm^{-1} in the fcc solid at 94 GPa and 300 K to less than 10000 Ω^{-1} cm^{-1} in the liquid at 470 K (91 GPa). This large drop is due to the combination of two effects, namely the decrease of the DOS and an increase in their localization near the Fermi level. To illustrate this, we have computed electron localization functions (ELF) [25]. The ELF's (Fig. 4B, Inset) indicate stronger electron localization in the broken symmetry phase compared with both the lower-pressure liquid and the finite-temperature fcc solid. We have also confirmed this by computing maximally localized Wannier functions [26], which exhibit decreased spread in the liquid above 65 GPa. Other unusual optical properties in this phase are likely as well. These findings could be confirmed by combined structure and conductivity measurements performed at modern synchrotron sources. We anticipate that our work will stimulate future experiments to confirm our predictions for sodium and to follow our suggestions for discovering similar behaviour in other dense liquid metals.

Methods summary

The electronic structure is computed using ab initio DFT calculations [27]. We use the Perdew, Burke & Ernzerhof (PBE) Generalized Gradient Approximation to the exchange and correlation potential and a 20 Ry planewave basis expansion. This level of accuracy allows for relatively fast calculations, while still reproducing the FLAPW bcc and fcc crystal equation of states [4] up to 120 GPa within a 1GPa error at the highest pressure, and the experimental phase boundaries between the bcc, fcc and the cI16 solids. The Troullier-Martins atomic pseudopotential includes the valence 3s electrons and nonlinear core corrections. The molecular dynamics trajectories are integrated using our implementation of the velocity Verlet algorithm in the Quantum Espresso package [28]. To obtain accurate melting temperatures, the equations of motion are integrated with a time step as small as 30 a.u. (40 a.u. is used after melting has occurred). The temperature is controlled through a Berendsen thermostat [29] with a relaxation time of

0.1 ps. The analysis of electronic properties is performed using the ABINIT package [30]. The 'heat-until-it-melt' approach is effective at pressures above 25 GPa, where melting leads to a densification of the structure. In that case melting is observed within a few picoseconds. Overheating effects are possibly present below 25 GPa as very long simulation times were necessary to melt the system (30 ps were necessary to melt the system at 20 GPas – 800K). Therefore, the data points corresponding to the liquid phase below 30 GPa on Fig. 1 should be considered as upper boundaries for the melting temperatures.

To detect fine features of the DOS and to converge the conductivity calculations, it is necessary to carry out a very careful **k**-point sampling of the Brillouin zone. Our results are obtained by performing calculations with 1000 **k** points on 108 or 128 atomic configurations taken from the FPMD simulations. For the FPMD simulations, on the other hand, a Γ-point only sampling is sufficient; as illustrated in Fig. 3A the resulting DOS profile is identical to that obtained from FPMD simulations carried out with an 8 **k**-point mesh. The comparison was established for two selected pressures at which fully independent molecular dynamics trajectories have been generated using either a single **k**-point (Γ or an 8 **k**-point sampling of the Brillouin zone (BZ). Both the structures and the electronic properties (melting temperature, local order, electronic densities of states, conductivities) were undistinguishable. All other simulations were then performed with the Γ- point only sampling of the BZ.

1. Neaton, J.B. & Ashcroft, N.W. Pairing in dense lithium. *Nature* **400**, 141 (1999).

2. Neaton, J.B. & Ashcroft, N.W. On the Constitution of Sodium at Higher Densities. *Phys. Rev. Lett.* **86**, 2830 (2000).

3. Hanfland, M., Syassen, K., Christensen, N.E. & Novikov, D.L. New high-pressure phases of lithium. *Nature* **408**, 174 (2000).

4. Hanfland, M., Loa, I. & Syassen, K. Sodium under pressure: bcc to fcc structural transition and pressure-volume relation to 100 GPa. *Phys. Rev. B* **65**, 184109 (2002).

5. Syassen, K., Simple metals at high pressure. *High-Pressure Phenomena*, ed. by Hemley, R. J., Chiarotti, G., Bernasconi, M., & Ulivi, L. (IOS Press, Amsterdam, 2002); and references therein.

6. Gregoryanz, E., Degtyareva, O., Somayazulu, M., Hemley, R.J. & Mao, H. Melting of Dense Sodium. *Phys. Rev. Lett.* **94**, 185502 (2005).

7. Jayaraman, A., Newton, R.C. & McDonough, J.M. Phase Relations, Resistivity, and Electronic Structure of Cesium at High Pressures. *Phys. Rev.* **159**, 527 (1967).

8. Boehler,R. & Zha, C.-S. Systematics in the melting behavior of the alkali metals from DAC measurements. *Physica B* **139-140**, 233 (1986).

9. Glotzel, D. & McMahan, A.K. Relativistic effects, phonons, and the isostructural transition in cesium. *Phys. Rev B* **20**, 3210 (1979).

10. Bonev, S., Schwegler, E., Ogitsu, T. & Galli, G. A Quantum Fluid of Metallic Hydrogen Suggested by First-Principles Calculations. *Nature* **431**, 669 (2004).

11. Correa, A., Bonev, S. & Galli, G. Carbon under extreme conditions: Phase boundaries and electronic properties from first-principles theory. *PNAS* **103**, 1204 (2006).

12. Sugino, O. & Car, R. Ab Initio Molecular Dynamics Study of First-Order Phase Transitions: Melting of Silicon. *Phys. Rev. Lett.* **74**, 1823 (1995).

13. Ackland, G.J. & McLeod, I.R.. Origin of the complex crystal structures of elements at intermediate pressure. *New J. of Phys*. **6**, 138 (2004); and references therein.

14. Zha, C.-S. & Boehler, R. Melting of sodium and potassium in a diamond anvil cell. *Phys. Rev. B* **31**, 3199 (1985).

15. Waseda, Y., *The Structure of Non-Crystalline Materials: Liquids and Amorphous Solids* (Mc Graw Hill, Tx, 1980).

16. Steinhard, P.J., Nelson, D.R. & Ronchetti, M. Icosahedral Bond Orientational Order in Supercooled Liquids. *Phys. Rev. Lett.* **47**, 1297 (1981).

17. Hernandez, E. R., & Iniguez, J. First Principles simulations on the nature of the melting line of sodium. *Phys. Rev. Lett.* **98**, 055501 (2007).

18. Gaspard, J.P., Pellegatti, A., Marinelli, F. & Bichara, C. Peierls instabilities in covalent structures I. Electronic structure, cohesion and the Z= 8-N rule. *Phil. Mag.* **77**, 727 (1998).

19. Bichara, C., Pellegatti, A. & Gaspard, J.P. Properties of liquid group-V elements: A numerical tight-binding simulation. *Phys. Rev. B* **47**, 5002 (1993).

20. Raty, J.Y. *et al*. Distance correlations and dynamics of liquid GeSe: An ab initio molecular dynamics study. *Phys. Rev. B*, **64**, 235209 (2001) and references therein.

21. Beister, H.J., Strössner, K. & Syassen, K. Rhombohedral to simple-cubic phase transition in arsenic under pressure. *Phys. Rev. B* **41**, 5535 (1990).

22. Chattopadhyay, T., Boucherle, J.X. & Von Schnering, H.G. Neutron diffraction study on the structural phase transition in GeTe. *J . Phys. C: Solid State Phys*. **20**, 1431(1987).

23. Katayama, Y. & Tsuji, K. X-ray structural studies on elemental liquids under high pressures. *J. Phys.: Condens. Matter* **15**, 6085 (2003).

24. Tamblyn, I., Raty, J.Y. & Bonev, S.A., unpublished.

25. Becke, A.D., Edgecombe, K.E. A simple measure of electron localization in atomic and molecular systems. *J. Chem. Phys.* **92**, 5397 (1990).

26. Marzari, N. & Vanderbilt, D. Maximally localized generalized Wannier functions for composite energy bands. *Phys. Rev. B* **56**, 12847 (1997).

27. Kohn,W. & Sham, L.J. Self-consistent equations including exchange and correlation effects. *Phys. Rev.* **140**, A1133 (1965).

28. S. Baroni *et al.* http://www.pwscf.org.

29. Berendsen, H.J.C., Postma, J.P.M, van Gunsteren, W.F., DiNola, A. & Haak, J.R. Molecular dynamics with coupling to an external bath. *J. Chem. Phys.* **81**, 3684 (1984).

30. Gonze,X. *et al*., First principles computation of material properties : the ABINIT software project. *Comp. Mat. Sci.* **25**, 478 (2002) ; www.abinit.org.

Supplementary Information accompanies the paper on **www.nature.com/nature**.

Acknowledgements The authors wish to thank Prof. Ivo Souza for fruitful discussions about the Wannier functions in a metal. This work was supported by the NSERC of Canada. J.Y.R. acknowledges support by the FNRS and the FAME NoE. E.S. worked under the auspices of the U.S. Dept. of Energy at the University of California/Lawrence Livermore National Laboratory under contract no. W-7405-Eng-48.

Authors contributions J.Y.R, E.S and S.A.B. contributed equally to this work. J.Y.R. and S.A.B designed the research. J.Y.R and E.S. conducted the molecular dynamics simulations. J.Y.R, E.S and S.A.B. performed the data analysis (S.A.B. and J.Y.R. computed the densities of states and conductivities; E.S. performed the Wannier analysis; J.Y.R. performed the model calculations and the ELF analysis; S.A.B. performed the solid state calculations).

Author information Reprints and permissions information is available at npg.nature.com/reprintsandpermissions. The authors declare no competing financial interest.

Correspondence and request for materials should be addressed to J.Y.R. (jyraty@ulg.ac.be) or S.B. (stanimir.bonev@dal.ca)

Figure 1. The melting curve of sodium under pressure. The theoretical results are shown in red: open and filled triangles indicate simulations of solid and liquid phases respectively. Data points of solid and liquid simulations on the same isochore that bracket the melting temperature are connected with lines. Experimental measurements are shown with diamonds [6] and with filled circles [14]. Inset: Evolution of the first peak maximum of $S(q)$ with pressure. Open circles are the theoretical results, diamonds indicate measurements [6], and the solid line is the bcc (100) peak position.

Figure. 2. Distribution of interatomic distances in Na as a function of pressure and temperature. (**A**) Pressure dependence of the average interatomic distances to the 1st, 2nd, 3rd, etc. nearest neighbours (n.n.) along the melting curve in liquid Na. Distances are scaled with respect to the 6th n.n. distance, r_6, in order to facilitate comparison at different densities. (**B**) Atomic arrangements in the fcc and bcc structures. The fcc cluster with 12 n.n. is almost identical to the bcc cluster composed of 8 n.n. (blue) and 4 next n.n. (grey); the 2 remaining next n.n. in bcc are shown in orange with dotted bonds.

(**C**) Probability distributions of the interatomic distances computed for model finite temperature fcc and bcc solids. Thermal disorder in the model structures is introduced by displacing the atomic positions according to a Gaussian distribution, $\delta x = \exp(-d_1^2/2\sigma^2)$. Here d_1 is the nearest neighbour distance in the 0 K crystal, and $\sigma = 0.1$ corresponds to the measured Debye-Waller factor in the simulated Na system (40GPa, 600K). Increased disorder (expressed in % of the 0K solid n.n. distance) corresponds to increased temperature. The validity of this approach is illustrated in the Supplemental Material.

Figure 3. Structure factors S(q) and electronic density of states (DOS) in solid and liquid Na as a function of pressure and temperature. (**A**) The bottom three curves are liquid S(q)'s computed at the following pressure and temperature conditions: 3GPa and 650K (grey line), 59GPa and 745K (dotted line) and 106GPa 500K (red colour). The upper three curves are computed S(q)'s of the following solid phases: bcc at 20 GPa and 700 K (grey line), fcc at 69 GPa and 500K (dotted line), and cI16 at 105 GPa and 200 K (red colour). In order to compare S(q)'s at different densities, the curves are scaled with respect to their first peak positions, q_1. The S(q)'s are computed by Fourier transforming (g(r)-1), where the g(r)'s are scaled to approach unity smoothly for r>15 a.u. Finite-size effects result in spurious oscillations for small q values, indicated with dashed lines in the figure. (**B**) At 39 GPa (bottom three curves), the DOS of the liquid is similar to that of the heated bcc solid and to the perfect bcc crystal. At 90 GPa (upper three curves), the liquid DOS exhibit a pseudogap, which is not present in the fcc solid at the same pressure but is similar to the pseudogap in the 0 K cI16 crystal. The dotted line is the DOS obtained from an MD simulation carried out with 8 **k**-points in the Brillouin zone; the agreement with the gamma-point only simulation is excellent. The inset shows the difference between the DOS of the liquid and solid near melting.

Figure 4. Physical origin and properties of the low-coordination phase of dense liquid Na. (**A**) Bottom: densities of *p* states in bcc and cI16 (with distortion parameter u=0.04; u=0 resulting in bcc) at 0GPa and 94GPa; and Top: *s*, *p* and *d* partial DOS in the 91GPa liquid (red) compared with the 0K fcc solid (green) and the heated solid (dashed black). (**B**) Electrical conductivity in liquid and solid phases of Na as a function of pressure. Inset: Differences, Δ in integrated Electron Localization Functions, ELF [24]. A higher ELF value indicates stronger electron localization, while a value of 0.5 corresponds to free electron behaviour.

Figure1

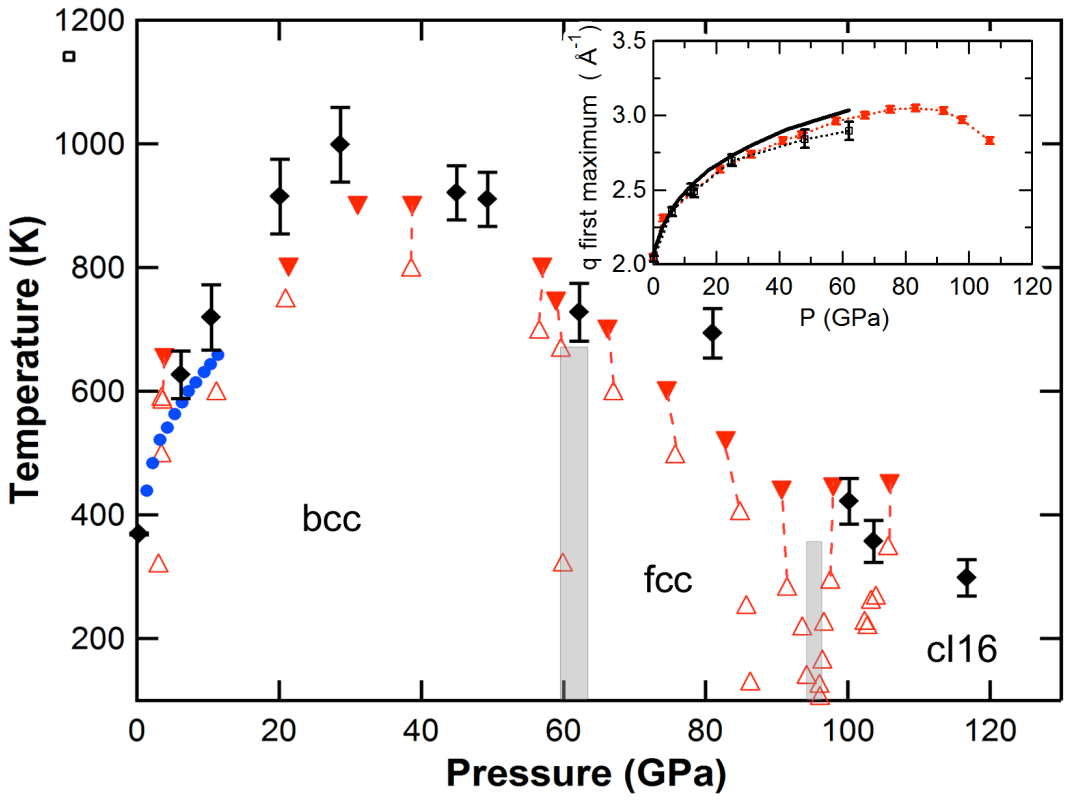
Temperature (K)
Pressure (GPa)
bcc
fcc
cl16
q first maximum (Å^{-1})
P (GPa)

Figure 2

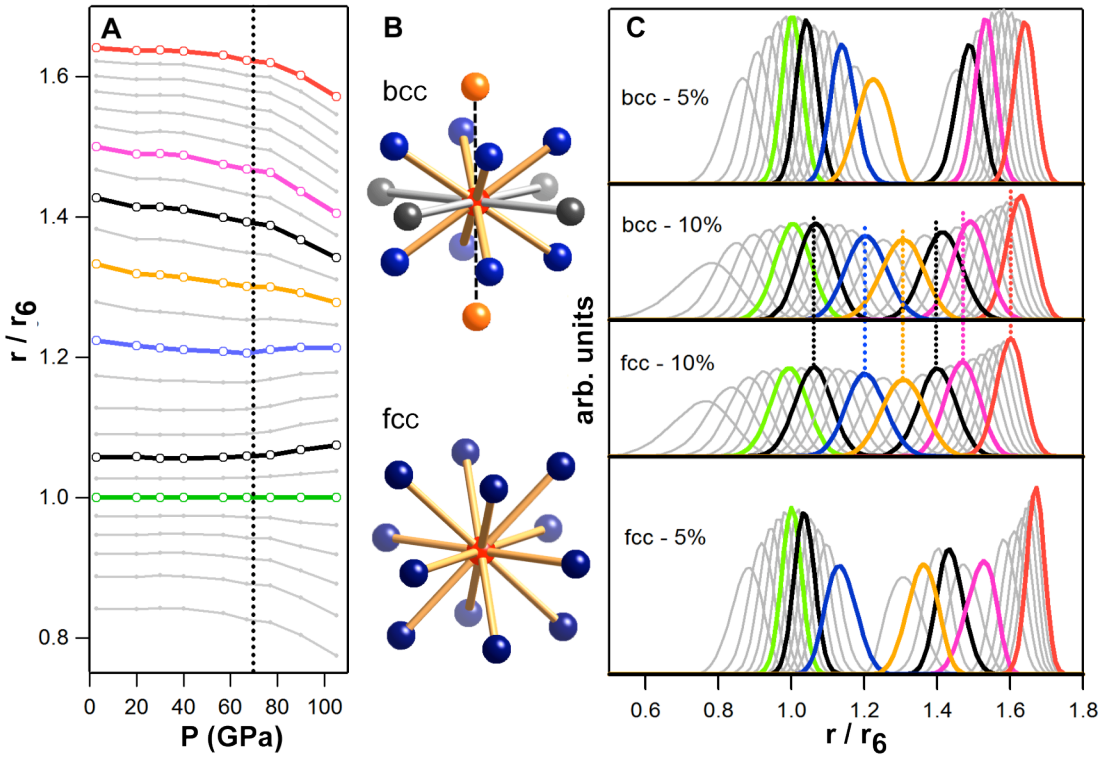
A
B
C
bcc
fcc
bcc - 5%
bcc - 10%
fcc - 10%
fcc - 5%
r / r6
P (GPa)
arb. units
r / r6
1.6
1.4
1.2
1.0
0.8
0
20
40
60
80
100
0.6
0.8
1.0
1.2
1.4
1.6
1.8

Figure 3

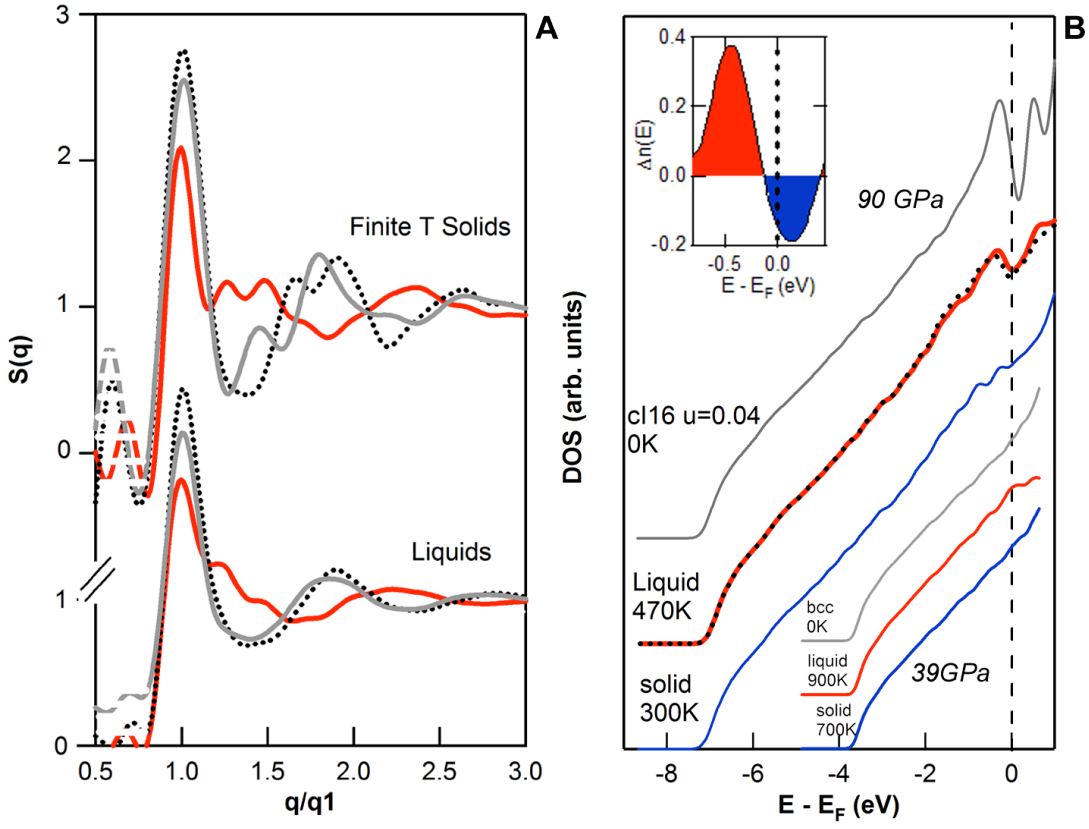
A
S(q)
q/q1
Finite T Solids
Liquids
B
DOS (arb. units)
E - E_F (eV)
Δn(E)
E - E_F (eV)
90 GPa
cl16 u=0.04
0K
Liquid
470K
solid
300K
bcc
0K
liquid
900K
solid
700K
39GPa

Figure 4

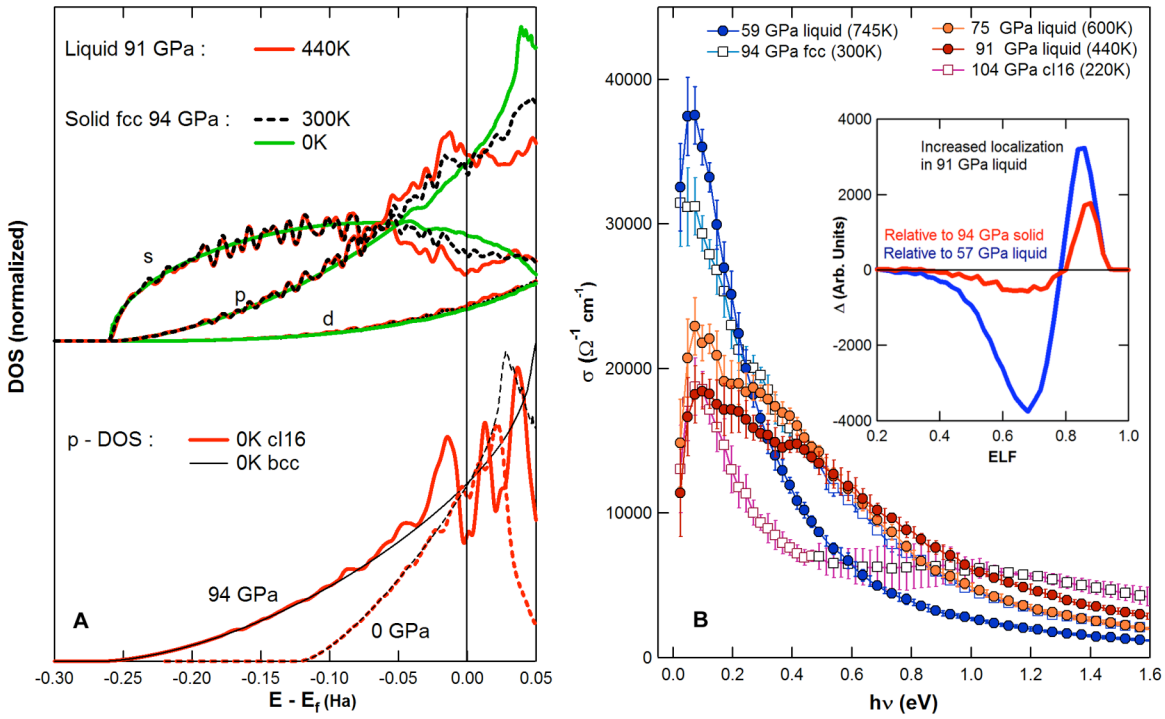
Liquid 91 GPa :
440K
Solid fcc 94 GPa :
300K
0K
s
p
d
p - DOS :
0K cI16
0K bcc
94 GPa
0 GPa
A
DOS (normalized)
E - E_f (Ha)
59 GPa liquid (745K)
94 GPa fcc (300K)
75 GPa liquid (600K)
91 GPa liquid (440K)
104 GPa cI16 (220K)
Increased localization
in 91 GPa liquid
Relative to 94 GPa solid
Relative to 57 GPa liquid
Δ (Arb. Units)
ELF
σ (Ω^-1 cm^-1)
hν (eV)
B